IEEE Access
Multidisciplinary | Rapid Review | Open Access Journal

IEEE POWER & ENERGY SOCIETY SECTION

Received 9 July 2024, accepted 11 August 2024, date of publication 15 August 2024, date of current version 27 August 2024.

Digital Object Identifier 10.1109/ACCESS.2024.3443917

RESEARCH ARTICLE

Detection and Location of Open Conductor Faults for Power Distribution Networks Using a Contingency Analysis Approach

GI-DO SIM, (Student Member, IEEE), HYO-SEOP IM, (Student Member, IEEE), JOON-HO CHOI, (Senior Member, IEEE), SEON-JU AHN, (Member, IEEE), AND SANG-YUN YUN, (Member, IEEE)

Department of Electrical Engineering, Chonnam National University, Gwangju 61186, South Korea

Corresponding author: Sang-Yun Yun (drk9034@jnu.ac.kr)

This work was supported in part by Korea Electric Power Corporation (KEPCO) through the KEPCO Research Institute under Grant R22DA08, and in part by the Regional Innovation Strategy (RIS) through the National Research Foundation of Korea (NRF) funded by the Ministry of Education (MOE) under Grant 2021RIS-002.

ABSTRACT This paper presents a method for the detection and location of open conductor faults (OCFs) in power distribution networks using contingency analysis (CA) based on unsymmetrical power flow calculations. The proposed method is designed for use in distribution management systems and broadly comprises two stages. The first stage is CA in study mode. This study presents a CA technique for detecting events different from those of the transmission network to evaluate network security. Accordingly, OCFs that can occur in the target network are analyzed using the unsymmetrical power flow method regarding the sections of the feeder remote terminal units (FRTUs), and the results are organized as a dataset for OCF CA (DOCA). The DOCA for the distribution lines (D/L) where topology changes have occurred is partially changed, and a detailed fault analysis is performed. The second stage is OCF detection and location in a real-time operating mode. This study proposes a method that compares the mean square error between real-time FRTU measurements and DOCA. The reliability of the proposed method is verified using MATLAB/Simulink to conduct various case studies on the IEEE 33 bus and 118 bus standard test models. The advantages of the proposed method can be summarized as follows: First, by comparing the distance between the entire set of measurements and DOCA, the proposed method achieves a considerably higher detection rate than those achieved by existing methods that use a single measurement element. Second, when calculating the distance between the two sets, the proposed method uses weights based on the magnitude variation of the comparison elements, which results in almost no false positives, making it robust to realistic conditions such as measurement sensor errors and communication delays. Third, fast responses during operations are also possible because detection and location are performed simultaneously.

INDEX TERMS Open conductor fault, contingency analysis, unsymmetrical power flow method, fault detection and location method, power distribution network.

I. INTRODUCTION

The extreme climate fluctuations caused by abnormal weather and global warming are causing severe socio-economic damage, including large-scale fires due to open conductor faults (OCFs) [1]. Furthermore, the detection and location of OCFs at power distribution networks are becoming increasingly complex because of various reasons, such as an accelerated connection of distributed energy resources (DERs), the expansion of covered lines and reinforced-concrete poles, and the use of various controllers for the efficiency of network operations.

The associate editor coordinating the review of this manuscript and approving it for publication was Sarasij Das.

In power distribution networks, faults have traditionally been detected on the basis of momentary fluctuations in the measurement values of field terminal units and protective equipment. However, OCFs are accompanied by dynamic changes after the instantaneous disconnection of conductors or connections. In addition, various fault behaviors (high-impedance faults, overcurrent faults, arcing, etc.) can occur depending on whether there is contact with a medium after the fault, which can lead to secondary damage such as fires and electric shock injuries. Therefore, there is a need for a detection and location technology that is specific to OCFs and different from existing methods.

Various studies have been conducted on OCF detection and location. First, attempts were made to detect OCFs using feeder remote terminal units (FRTUs) and their measurement values [2], [3], [4], [5], [6]. A voltage-based OCF detection method using voltage outage [2] and OCF detection methods using the current unbalance of negative-sequence current compared to positive-sequence current were proposed [3], [4]. These deterministic detection methods have the advantage of easy applicability to actual networks because the fluctuations of a certain element are set as the detection criteria; however, they are unavoidably influenced by the network environment and fault location. To resolve these problems, detection methods utilizing multiple detection elements as open fault condition (OFC) were proposed [5]. However, this approach has the limitation of being vulnerable to any increase in the DER connection and end-of-line faults that produce little fluctuation. A method was proposed to calculate the impedance during low-impedance ground fault (LIGF) and high-impedance ground fault (HIGF) conditions after OCF. This impedance was then reflected in the operating range of distance relays for detection [6]. This method has limitations in that because of the range of fault impedance considered, it cannot consider dynamic changes in the OCF aspect.

Second, studies were conducted on primary detection using field-installed devices and determining final location either by collecting data from these devices in the distribution management system (DMS) or via communication between them [7], [8], [9], [10]. Research was conducted on methods that detect OCFs using voltage outage information from feeder-end voltage sensors and identify fault sections by topology analysis [7]. A method was proposed to detect OCFs by measuring voltage unbalance with smart meters at the end of a line and identifies the fault section by a common path search between detection devices [8]. Furthermore, a method was proposed to detect faults from the voltage unbalance in the secondary side of the distribution transformer and identify OCF locations via device-to-device communication [9]. In addition, a method was proposed to detect OCFs by calculating transient zero-sequence admittance at the FRTU and fault location from the difference in zero-sequence admittance at the source- and load-side of the fault point [10]. These methods have the same limitations as the abovementioned methods because they use certain detection elements of field devices, and they are unable to consider the effects of false positives (FPs) and false negatives (FNs) in field devices when the DMS determines the final location.

Third, OCF detection research was also conducted using artificial intelligence [11], [12], [13], [14]. One proposed method used an artificial neural network-based algorithm to learn actual faults and the voltage and current of an EMTP model and made comparisons with relay measurement values [11]. Another method performed detection by removing voltage and current noise and learning features by the discrete wavelet transform [12]. Further, a technique that extracted fault features using the variational mode decomposition technique and ultimately determined faults via a support vector machine was also presented [13]. Another study performed detection by using deep learning to extract voltage and current features from the frequency band directly after OCFs and applied them to a field phasor measurement unit [14]. In addition, a method that extracted features from sensor signals and detected faults using a graph-embedded low-rank tensor learning machine was proposed [15]. In another study, the characteristics of three-phase current waveform data were analyzed using convolutional neural networks to estimate the type, phase, and location of faults, including high-impedance faults [16]. The abovementioned methods perform learning using instantaneous value-based data; however, they are not realistic because the historical stored data of the actually operating DMS is based on root-mean-square values. In addition, there is a problem in that the detection criteria can vary according to the environment of the target network.

Fourth, studies were conducted on the detection and location of OCFs by contingency analysis (CA) [17], [18]. One proposed method calculated the Thevenin equivalent impedance for each symmetrical component assuming a single-phase OCF in a line section and used the load-side zero-sequence component current fluctuation rate for the assumed substation secondary-side zero-sequence component voltage as the detection criterion [17]. This method is limited by the problem of setting the voltage fluctuation criterion and the fact that it requires a measurement environment that guarantees simultaneity. Further, a method that estimated the voltage of fault candidate points and ultimately performed power flow calculations to select the final fault locations as the locations with the smallest deviation between the measured voltage and the calculated voltage at the substation secondary side was also studied [18]. This method can be applied to common network topologies but has problems in that it does not consider DER and takes a long time to determine the location because of its repeated power-flow calculations.

To summarize the above literature review, methods that are based on field devices and methods that make a final OCF decision and perform location via cooperation between field devices and DMS have problems in that their detection criteria are set according to the target network and they are

vulnerable to operational noise (FPs, FNs, communications delays and failures, etc. in field devices). Methods that use CA have problems in that they do not consider the various OCF behaviors, can only be applied to certain network topologies, and do not have a clear basis for setting the detection criteria. In addition, only methods that apply to real-time operational situations are mentioned, and insufficient consideration is given to the time spent and computations performed by DMSs that manage hundreds or thousands of distribution lines (D/Ls).

To resolve these problems, this paper proposes a real-time OCF detection and location method that performs offline CA, which considers various behaviors of OCF and compares the results with real-time FRTU measurement values. CA, which is a detailed fault-analysis method that requires considerable computation and time, is performed separately offline. During real-time operations, OCF detection and location are performed by comparing the mean squared error (MSE), considering the FRTU measurement error. The contributions of this paper can be summarized as follows:

1) A CA method based on an unsymmetrical power flow method is proposed, considering OCF characteristics and DERs. To overcome the limitations of certain detection elements, CA is employed to detect fluctuations in voltage, current, and power factor (PF) angle, which are organized into a dataset for OCF CA (DOCA). By comparing DOCA with the overall measurement set, the detection rate of the proposed method is significantly higher than those of existing methods using a single measurement element.

2) When comparing the distance between the FRTU measurement set and DOCA, the proposed method applies weights based on the magnitude variation of comparison elements (calculated in advance), thus resulting in almost no FPs. The measurement error of sensors and the sensitivity are also analyzed in advance, thereby affording OCF decision and location criteria suitable for the network. Therefore, the method is robust to realistic conditions, such as measurement errors and communication delays that may occur in the operation of the distribution system.

3) The dataset of DOCA is composed of the values of measurement elements when OCF occurs in a specific section. Detection and location are performed simultaneously when determining the event by a comparison with the measurement values of FRTU, which enables quick response during operation.

4) The proposed method of performing CA along with detection and location of OCFs uses only data and measurement infrastructure that are commonly possessed by most power companies today. Therefore, this study is highly applicable to actual network operations.

The remainder of this paper is organized as follows. Section II analyzes the characteristics of OCFs. Section III describes the CA-based OCF detection and location algorithm. Section IV verifies the algorithm by case studies. Finally, Section V concludes this paper.

II. OCF CHARACTERISTIC ANALYSIS AND REVIEW OF PREVIOUS STUDIES

OCFs occur because of factors such as mechanical impacts from the external environment, mechanical defects in connections, and corrosion due to deterioration; they are defined as unintentional single-phase or double-phase openings in energized conductors. In OCFs, the measurement values of FRTUs fluctuate during faults because of two reasons:

1) Changes in the fault itself: In an OCF, the conductor itself is mechanically separated. Therefore, the aspects of the OCF can dynamically change, commencing directly after the fault. As such, OCFs cannot simply be defined as openings in an electrical circuit but can be broadly classified according to three aspects: (1) a high-resistance state is maintained, in which the power line does not contact a low-resistance medium after the fault; (2) a separated power line contacts a low-resistance medium such as the earth or a pole, and the fault changes into a ground fault (GF); (3) the situation changes into an OCF after the GF occurs.

2) Fluctuations in measurement values due to the network structure: If an OCF occurs in a power distribution network that comprises simple loads, the voltage fluctuations on the source side of the fault point are minimal, and the current is affected by the load drop caused by the fault [2], [4]. However, various voltage and current fluctuations can occur on the load side of the fault point depending on the transformer connection [5]. When a Δ load is connected to the primary-side Δ connection transformer and the Yg-Yg connection, it acts as the current source after the OCF occurs, and a voltage close to a maximum of 0.5 pu can be maintained. However, the maintained voltage can fluctuate because of the internal voltage drop caused by the load current. In the case of a Yg-Δ connection to supply an industrial high-voltage customer (using a motor) or a transformer to connect a DER, a maximum voltage of 1.0 pu can be maintained. The voltage and current fluctuation patterns vary because of the distribution of the load and the amount of distributed generation below the fault point due to the transformer connection.

To determine whether an OCF has occurred, it is necessary to detect instantaneous changes. Therefore, OCF detection methods that use fluctuations in the measurement values of field terminal devices have traditionally been employed. Typical examples of these include a method that uses current unbalance (the ratio of the positive phase sequence component to the negative phase sequence component) changes [3], a method that detects OCFs by combining multivariate detection elements into a decision tree [5], and methods that detect OCFs using voltage drop and voltage unbalance and determine the locations of the OCFs by a path search [7], [8]. To examine the limitations of existing OCF detection methods, the test power distribution network shown in Fig. 1 was used. In Fig. 1, the impedance of M.Tr. is 30% based on 100 MVA, and each load is assumed to be 0.5 MVA (lagging PF of 0.95). The distribution transformer for the load is 6% of 1-MVA capacity, and Yg-Yg and Δ-Yg connections

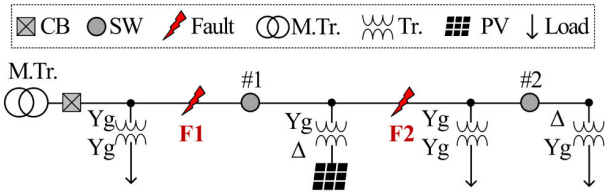

FIGURE 1. Test network for a comparison of previous studies.

TABLE 1. Comparison of OCF detection methods using FRTU measurement values.

Method	Fault	FRTU	Results	Detection criteria
[3]	F1	CB	**0.95/42.75 = 3.8 %**	$\frac{I^{(2)}}{I^{(1)}} > 15\ \%$
	F2	CB	9.89/16.22 = 61.0 %	
		SW #1	5.55/9.91 = 56.1 %	
[5]	F1	CB	OFC_4 & OFC_5	Multivariate OFCs
		SW #1	**Undetected**	
		SW #2	**Undetected**	
	F2	CB	OFC_4 & OFC_5	
		SW #1	OFC_2 & OFC_3	
		SW #2	OFC_2 & OFC_3	
[7]	F1	SW #1	**ΔV= 0.2%**	$\Delta V > 30\ \%$
		SW #2	**ΔV= 9.2%**	
	F2	SW #2	ΔV= 80.1%	
[8]	F1	SW #1	**V_{ub}= 3.7 %**	$V_{ub} > 30\ \%$
		SW #2	**V_{ub}= 3.6 %**	
	F2	SW #2	V_{ub}= 66.5 %	

*OFC2: Voltage outage ($V_{OT} > 50\%$), OFC3: Current outage ($I_{OT} > 50\%$)
*OFC4: Change of impedance ($|\Delta Z > 20\%$), OFC5: Change of current ($|\Delta I > 20\%$)

are assumed. The capacity of photovoltaics(PV) is set at 0.5 MW and connected as Yg-Δ. The line is ACSR 160 mm^2 and has a total length of 5 km. The fault simulated a situation in which a high resistance was maintained after the OCF, and the fault locations were set as the source and load sides with the PV. Table 1 compares the detection results of each of the existing methods when an OCF occurs. In the case of fault location "F2", all methods succeeded at OCF detection; however, in the case of fault location "F1", there were some detection failures. Fault location "F1" revealed that FNs occurred because there was little fluctuation in the detection elements (Table 1) due to the effect of the voltage source that was maintained by the DER connection transformer below the fault point.

In this paper, field measurements and analytical situation predictions are compared to resolve the problems in previous studies that depended solely upon measurement values for OCF detection. CA is a method for making analytic situation predictions regarding power networks. The CA that is used in transmission network operations has been employed to evaluate the operating vulnerabilities of the current situation by implementing a power flow method assuming the occurrence of single or multiple network faults and the situations that occur after they are removed. Because the fault in the distribution network has a small impact, research has been conducted on using it to plan objectives for certain target networks rather than real-time operations. Lin et al. presented an optimal

TABLE 2. Fluctuation in voltage and current measurements due to a change in PV output and load demand.

Transformer capacity	V (pu) at the interconnection due to PV output		
	0%	50%	100%
1 MVA	0.901	0.908	0.915
2 MVA	0.944	0.948	0.953
FRTU	ΔI (%) due to load demand variations		
	30 %	60 %	100 %
CB	67.1	66.6	66.5
FRTU #1	99.8	99.7	99.6
FRTU #2	80.9	80.4	80.1

connection feeder investment and radial feeder operation plan based on N-1 CA to examine security when expanding power distribution networks [19]. Zou et al. presented a method that performed N-1 CA to examine the capacity limits of main transformers and connection lines and find vulnerable connection points during power distribution planning [20].

However, the detection of certain faults such as OCFs is becoming increasingly difficult because of increasing operational complexity caused by the increase in DER connections; therefore, the need for CA and its application in real-time operations is emerging. Real-time OCF detection that is based on contingency analyses of power distribution networks may encounter problems in terms of the computation and analysis time. In general, the number of D/Ls that are managed by a single distribution control center range from at least several hundred to over a thousand. Therefore, performing a detailed analysis for each contingency case requires an enormous amount of computation and time and is almost impossible to perform during real-time operations. Accordingly, it is necessary to separate time slots for analysis and the use of analysis results. However, this process also has a problem in that the network situation during analysis, specifically the load and PV generation, may differ from the real-time operational situation. To examine how this problem affects OCF detection, the fluctuations of voltage and current measurement are simulated according to the DER output and load demand fluctuations in the network shown in Fig. 1. Table 2 presents the results when the same OCF as that presented in Table 1 is simulated in fault location "F1". As revealed by Table 2, changes in PV output did not have a significant effect on voltage fluctuations, and the current fluctuation rate according to load demand fluctuation was not large either. Thus, a method that performs CA using only the static information that is possessed offline and applies the results to real-time operations can be proposed.

III. CONTINGENCY ANALYSIS-BASED OCF DETECTION AND LOCATION ALGORITHM

A. OVERALL STRATEGY

The overall strategy for OCF detection and location is presented in Fig. 2. As shown in Fig. 2, the proposed method comprises two stages: (1) a stage that creates a DOCA, which is a comparison dataset for OCF detection, by CA in a study mode, (2) a stage that performs OCF detection and location

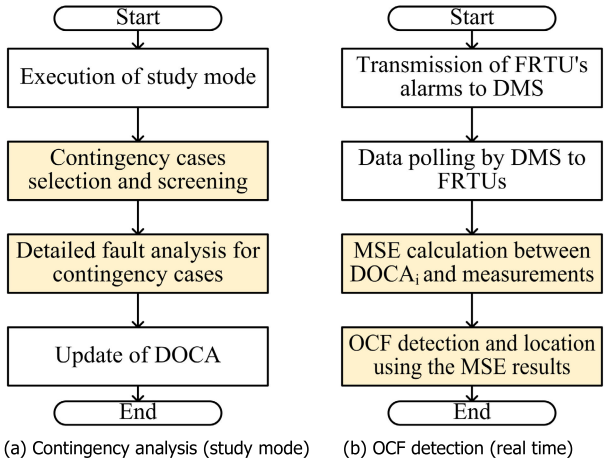

FIGURE 2. Overall flowchart of the proposed OCF detection and location strategy.

by comparing the minimum MSE of the DOCA and the measurements of FRTUs in a real-time operation mode. The summary of each process is as follows:

1) CA stage: The processes are aperiodically or periodically performed in study mode using the static data possessed by the power company and the present topology data at the time it is performed; the results of performing these processes are stored in the database of DMS for real-time operations. During the initial startup of the system or database update, all cases are generated; in addition, a contingency case selection and screening (CCSS) process is performed for the D/Ls with topology changes. In the contingency cases produced by the CCSS process, a single-phase OCF in an N-1 contingency situation is assumed for each type for all FRTU sections of each of the D/Ls. FRTU measurements are predicted for each fault case by a detailed fault analysis of each contingency case. Each FRTU measurement that is calculated for the i-th fault is defined as (1):

$$DOCA_i = \left\{V_{i1}, I_{i1}, \theta_{i1}, \ldots V_{ij}, I_{ij}\, \theta_{ij}\right\} \tag{1}$$

where V, I, and θ are the voltage, current, and PF angle measurement values of the j-th FRTU. Fault analysis is repeated for the n contingency cases derived from CCSS, and the results are stored in the memory database of the operating system.

2) OCF detection and location stage: The processes are performed if an event detection alarm occurs in one or more FRTUs during real-time operations. The DMS uses data-polling commands to collect the present FRTU measurements from the D/L where the alarm occurred. The MSE between $DOCA_i$ and the present measurement dataset is calculated by a Euclidean distance comparison between the calculated value of the j-th measurement of $DOCA_i$ and the present measurement of the j-th FRTU. The DMS data polling of the FRTUs to apply the proposed method may have a problem of FPs or FNs due to changes in the fault behavior. To resolve this problem, a fault analysis based on the situation after the OCF behavior changes is performed. In the case of a GF after an OCF, a fault analysis is performed using a power flow method for a situation that reflects both disconnections and GFs in the fault model, and the same procedure is performed for an OCF after a GF. By comparing the CA results and measurement values after all aspect changes were complete by data polling, this study aims to mitigate the problem of FPs and FNs. Finally, when the MSE is lower than the detection criterion, an OCF is detected, and its location is estimated by minimum MSE estimation.

B. PERFORMING CA AND CREATING DOCA IN STUDY MODE

The proposed OCF CA is divided into the process of screening and selecting OCF contingency cases and the process of creating the DOCA by detailed fault analysis. CCSS is performed to derive the contingency cases, which are the targets of the detailed fault analysis; this process is shown in the flowchart in Fig. 3. This process is performed using a breadth-first search of the target D/Ls [21]. First, the network data are read by finding all D/Ls when CCSS is initially performed or the relevant D/Ls when a topology change has occurred. In the case of an OCF, changes in the fault location between the measurement equipment on both the source and load sides do not have a significant effect on measurement values. Therefore, contingency case selection is performed using sections consisting of FRTUs. To achieve this, the lines and switches (SWs) are searched starting at the substation secondary-side breaker. In the case of the lines, the search continues, and in the case of the SWs, the section between two SWs is designated as a contingency case. If the path ends

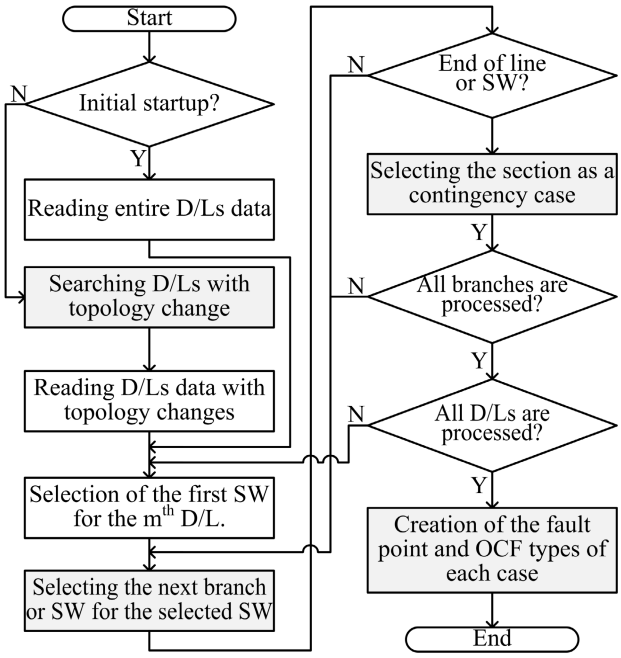

FIGURE 3. Flowchart of contingency case selection and screening.

after an SW, that section is designated as a contingency case. If there are no more lines or D/Ls to search, the process is finished, and fault points are designated within the line sections of the contingency case. The final contingency cases are generated by making assumptions about the OCF behaviors at the designated fault points. The final contingency cases store the information given by (2):

$$case_{m,i} = \{FN_{m,i}, FT_{m,i}\} \tag{2}$$

where $case_{m,i}$ is the i-th contingency case of the m-th D/L, $FN_{m,i}$ is the faulted node of that case, and $FT_{m,i}$ is the OCF behavior. For a detailed analysis, previous studies used a method that calculated the zero-sequence fault voltage and current using a voltage and current relational formula based on the equivalent impedance for each sequence [18] and a method that estimated voltage using the power flow method starting at the fault point [19]. Nevertheless, these methods have problems in that they do not reflect the control characteristics of DERs during faults and do not consider the various OCF behaviors. Grainger et al. presented an OCF analysis method that used the Thevenin equivalent resistance in a situation where one or two phases are connected in a three-phase open situation [22]. However, this method is difficult to apply to power distribution systems in which DERs and loads are dispersed. In the present work, detailed fault analysis is performed using an unsymmetrical three-phase power flow method that reflects the control characteristics of the power-conversion device of DER during faults and the various behaviors of OCFs and can also consider the characteristics of distributed loads and their connection transformers [23]. Fig. 4 shows the flowchart of the detailed fault analysis, which comprises the following steps:

① Selecting the contingency case: The contingency cases that were previously selected via CCSS are selected, and a fault model is applied according to the fault type. In this work, several fault models are used. First, when a high resistance is maintained after the OCF, it is modeled as an infinite impedance inserted in the faulty line in a series. Second, cases of GFs after OCFs are divided into source- and load-side GFs. To model the open conductor itself, an infinite impedance is inserted in series, and it is modeled in the form of the source- and load-side nodes grounded with a fault point resistance. Third, the case of an OCF after a GF is a situation in which a GF occurs because of contact with objects such as trees and then changes into an OCF owing to a physical impact. Such faults are modeled in the same way as when a high resistance is maintained after an OCF, but it is assumed that protective equipment is operating near the GF fault point and the load-side DERs of the fault point are eliminated (due to low voltage).

② Creation of the Z_{bus} matrix for the selected case: The network admittance data and the fault model of the contingency case are applied to create an admittance matrix for the three-phase unsymmetric power flow method. Finally, this matrix is inverted to create the impedance matrix.

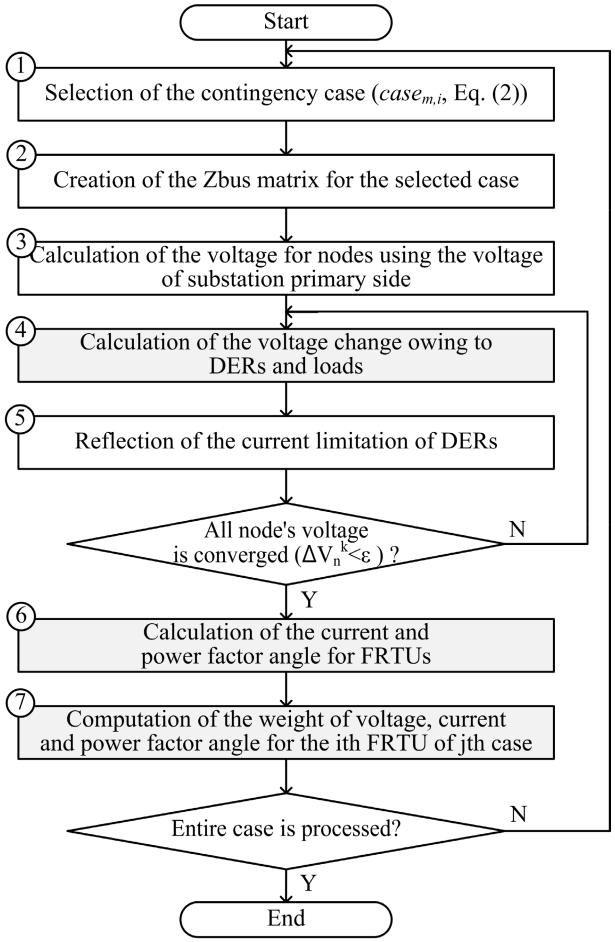

FIGURE 4. Flowchart of the detailed fault analysis for the contingency.

③ Calculation of the voltage for nodes using the voltage of the substation primary side: To do so, the current is calculated by only activating the voltage source of the substation (slack bus) in a state where the distribution generator and load are open, and the voltage of each node is calculated using the calculated current as given by (3):

$$\begin{bmatrix} V_{s,1} \\ V_{s,2} \\ \vdots \\ V_{s,n} \end{bmatrix} = \begin{bmatrix} Z_{11} & \cdots & Z_{n1} \\ \vdots & \ddots & \vdots \\ Z_{1n} & \cdots & Z_{nn} \end{bmatrix} \begin{bmatrix} I_s \\ 0 \\ \vdots \\ 0 \end{bmatrix} \tag{3}$$

where I_S is the current vector that flows from the substation, Z_{nn} is the network impedance matrix, and V_s is the voltage vector due to the voltage source at the substation side.

④ Calculation of the voltage change due to DERs and loads: The substation node is eliminated, and the voltage fluctuation in a situation in which only the DER and load are connected is calculated using (4):

$$\begin{bmatrix} \Delta V_1^k \\ \Delta V_2^k \\ \vdots \\ \Delta V_n^k \end{bmatrix} = \begin{bmatrix} Z_{11} & \cdots & Z_{n1} \\ \vdots & \ddots & \vdots \\ Z_{1n} & \cdots & Z_{nn} \end{bmatrix} \begin{bmatrix} 0 \\ I_2^k \\ \vdots \\ I_n^k \end{bmatrix} \tag{4}$$

where k is the iteration number of power flow calculation. I^k is the network current vector and is calculated by dividing the DER current and the load current values by the corresponding node voltage. ΔV^k is the voltage vector change due to DER. Next, ΔV^k is added to calculate the voltage using (5):

$$\begin{bmatrix} V_1^{k+1} \\ V_2^{k+1} \\ \vdots \\ V_n^{k+1} \end{bmatrix} = \begin{bmatrix} V_{s,1} \\ V_{s,2} \\ \vdots \\ V_{s,n} \end{bmatrix} + \begin{bmatrix} \Delta V_1^k \\ \Delta V_2^k \\ \vdots \\ \Delta V_n^k \end{bmatrix} \tag{5}$$

where V^{k+1} is the node voltage vector.

⑤ Reflection of the current limitation of DERs and whether the voltage has converged: The DER output current is calculated using the connection point voltage. It is determined whether this current exceeds the maximum current. If the DER current is greater than the limit value, the current is limited as given by (6):

$$I_{DG} = \begin{cases} \dfrac{S_{DG}}{V_{DG}} & \dfrac{S_{DG}}{V_{DG}} < I_{DG,max} \\ I_{DG,max} & \dfrac{S_{DG}}{V_{DG}} \geq I_{DG,max} \end{cases} \tag{6}$$

where I_{DG} is the DER output current, V_{DG} is the connection point voltage, and S_{DG} is the DER supplied power. $I_{DG,max}$ is the maximum current limit according to the power-conversion equipment capacity. If the current of all DERs is less than the limit value, a decision is made regarding whether the voltage has converged. If it has not converged entirely, the process returns to ④ and repeats.

⑥ Calculating the voltage, current, and PF angle of the FRTU installation point: The voltage and phase of each node are estimated using the power flow method, and then the current and PF angle of the FRTU installation points are calculated. The current is calculated using the voltage at both ends of the FRTU and the three-phase line impedance between them, and the PF angle is calculated using the voltage and the current phase.

⑦ Computing the weights for the voltage, current, and PF angle: There are differences in the amounts of fluctuation in the voltage, current, and PF angle according to the OCF fault type and detection location. When the OCF decision is made by comparing the DOCA set and the current measurement values presented in Section III-C, weights are assigned according to the amount of fluctuation to prevent bias in the results for variables with small amounts of fluctuation. Equation (7) expresses the fluctuation calculation for calculating the weights:

$$\Delta k_{i,j}(PU) = \frac{|k_j - k_{i,j}|}{k_j} \tag{7}$$

where $\Delta k_{i,j}$ is the amount of fluctuation in each measurement element ($k = V; I; \theta$), and it indicates the i-th case, j-th FRTU voltage, current, and PF angle. k_j and k_{ij} are the analysis values of each measurement element of the FRTU before and after the i-th OCF occurs, respectively. The weights are calculated using the relevant values as given by (8):

$$\omega_{V_{i,j};I_{i,j};\theta_{i,j}} = \frac{\Delta V_{i,j};\ \Delta I_{i,j};\ \theta_{i,j}}{\Delta \mathrm{V}_{i,j} + \Delta I_{i,j} + \Delta \theta_{i,j}} \tag{8}$$

where $\omega_{V_{i,j}}$, $\omega_{I_{i,j}}$, and $\omega_{\theta_{i,j}}$ are the voltage, current, and PF angle weights of the j-th FRTU of the i-th CA results, respectively.

The fault analysis results are used to create the DOCA and stored in the database for DMS operations. Fig. 5 shows an example of the DOCA database. The DOCA comprises three tables: D/Ls, FRTUs, and fault analysis results. The D/L table stores information on the number of FRTUs and contingency cases, and the FRTU table stores information on the affiliated D/Ls. The fault analysis results table stores the FRTU measurement values that were analyzed for each contingency case of D/L.

DL

ID	NO of FRTUs	NO of CASEs
DL#1	i	l
DL#2	j	m
⋮	⋮	⋮
DL#n	k	n

FRTU

ID	DL_ID
FRTU#1	DL#1
FRTU#2	DL#1
⋮	⋮
FRTU#n	DL#n

Fault analysis results

DL_ID	CASE_ID	FRTU_ID	DL#1_V	DL#1_I	•••	DL#n_I	DL#n_θ
DL#1	CASE#1	FRTU#1	θ#1	I#1	•••	NULL	NULL
DL#1	CASE#1	FRTU#2	θ#2	I#2	•••	NULL	NULL
DL#1	CASE#1	FRTU#3	θ#3	I#3	•••	NULL	NULL
⋮	⋮	⋮	⋮	⋮		⋮	⋮
DL#n	CASE#n	FRTU#n-1	NULL	NULL	•••	I#n-1	θ#n-1
DL#n	CASE#n	FRTU#n	NULL	NULL	•••	I#n	θ#n

FIGURE 5. Overall database of DOCA for OCF detection and location.

C. OCF DETECTION AND LOCATION IN REAL-TIME OPERATION MODE

The OCF detection and location process consists of FRTU event detection, polling the present data of the FRTUs of the relevant D/Ls, calculating error by a comparison of the DOCA and the present measurement data, and deriving conclusions. The flowchart for this process is shown in Fig. 6 and described in detail below:

1) FRTU event detection and collection: Collection of FRTU data by the DMS is broadly divided into periodic/aperiodic data polling and aperiodic report by exception (RBE). RBE is a method in which the FRTU transmits signals without a request by the DMS when an event occurs. In this study, the FRTU alarm is used for suspected abnormal situations as a preprocessing step for OCF detection. To implement the preprocessing step, the voltage fluctuation ($\Delta V_{x-cycle}$) and current unbalance ($\Delta I_{ub\_x-cycle}$), which commonly occur in almost all abnormal network situations, are used. In the IEEE C57.13 and IEC 61869 protection

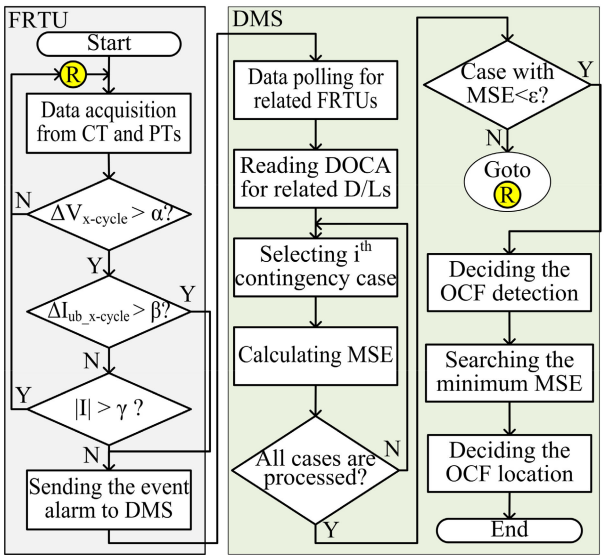

FIGURE 6. Overall flowchart of the OCF detection and location strategy.

class 3 standards, the voltage error is defined as 3%, and in IEEE 1547, the instantaneous voltage fluctuation rate due to DERs is limited to 3% [24], [25], [26]. Therefore, in this work, the value of the voltage error plus the voltage fluctuation rate is set as the minimum criterion (α) for event detection. The current unbalance criterion (β) is based on a previous study [3]. The suspected abnormal situation alarm uses the information detected by the FRTU in a high-impedance state immediately after OCF occurs. In the case of an OCF after a GF, an alarm does not occur in the FRTU in cases accompanied by an overcurrent ($\Delta |I| > \gamma$) to avoid using information that is detected in situations that are not high-impedance states.

2) DMS data polling: If an event is detected, the present measurement values of FRTUs for the relevant D/Ls are collected via polling commands from the DMS. In the duration in which the polling command and data collection are carried out, the fault behavior changes, and stabilization is performed to change to a state in which fixed measurement values are maintained. In the case of an OCF after a GF or a GF after an OCF, protective equipment may operate because of an overcurrent. However, in an overcurrent situation in the case of an OCF after a GF, an alarm does not occur. Therefore, the polling command is executed after the protective equipment recloses. In the case of a GF after an OCF, there is time to change to a GF and for the protective equipment to operate. Therefore, the measurement values can be collected in a state where fixed measurement values are maintained.

3) Fault detection and location: The data that were previously collected via data polling are compared with the DOCA results that were stored in advance. The DOCA stores the calculation datasets for each OCF type, and the present FRTU measurement values are compared with all presumed fault types. The stored dataset of GF faults after OCFs in DOCA is compared with the present load-side measurement values of FRTUs in the case of source-side GFs or the present source-side measurement values of FRTUs in the case of load-side GFs. In the case of GFs, the changes in the magnitude of current according to the fault point resistance are relatively large. Therefore, comparisons are only made between values for the load-side of the faulted point, which are not affected by overcurrent. The comparison of the DOCA data and the present measurement data is obtained using (9):

$$d_{k,ij} = \frac{|k_{j,Meas}(t_j) - k_{i,j}|}{k_{j,Meas}(t_j)} \tag{9}$$

where $d_{k_{i,j}}$ is the error (pu) that is found by dividing the Euclidean distance between the measurement values of FRTU and the estimation values (CA results) of DOCA by the measurement values, and $k_{j,Meas}(t_p)$ are the measurement values of the j-th FRTU, which are measured and sent after the data-polling command. t_j is the time taken for the j-th FRTU to receive the data polling and transmit the measurement values to the DMS. Finally, the MSE is found from the Euclidean error and weights as given by (10), and detection and location are performed:

$$d_i = \frac{\sum_{j=1}^{n} \sqrt{\left(\omega_{V_{i,j}} d_{V_{i,j}}\right)^2 + \left(\omega_{I_{i,j}} d_{I_{i,j}}\right)^2 + \left(\omega_{\theta_{i,j}} d_{\theta_{i,j}}\right)^2}}{n} \tag{10}$$

where d_i is the MSE value (pu) of the Euclidean distance error of the voltage, current, and PF angle, and n is the total number of FRTUs. Finally, an OCF is decided to have occurred if there is a case that satisfies the condition given by (11):

$$d_i < \varepsilon, \quad i = 1, 2, \ldots..m \tag{11}$$

where m is the total number of contingency analyses, and ε is the detection criterion. The minimum criterion is chosen according to the voltage and current measurement error of the FRTU, and then it is set up considering the margin. If the minimum MSE is greater than the criterion value, it means that the event does not fully match the contingency case analysis results of the relevant D/L, and it is decided as ''OCF not detected.'' If there are one or more cases in which the MSE is less than the criterion value, it is decided as ''OCF detection.'' Finally, the fault location is estimated by estimating the minimum MSE. If there is one case that satisfies the condition given in (10), the FN_{mi} of that case is estimated as the fault location. If there are two or more cases, the FN_{mi} with the minimum MSE is estimated as the final fault location; this can be expressed as (12):

$$FN_{OCF} = argmin(d_i\left(FN_{m,i}\right)) \tag{12}$$

where FN_{OCF} is the location where the first-priority fault occurred. In the case of OCFs, there is no significant difference according to the section during fluctuation, Therefore, if second- and third-priority FN_{mi} are designated, the field crew can respond quickly if an OCF is not found at the first-place location.

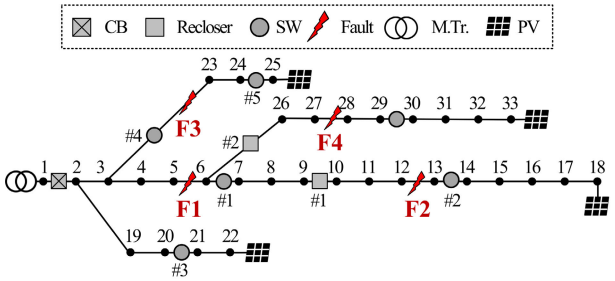

FIGURE 7. Modified IEEE 33 bus test system.

IV. CASE STUDIES

Case studies were performed on the proposed contingency analysis-based OCF detection and location method using modified IEEE 33 bus and 118 bus test networks [27], [28]. The procedure for the case studies is summarized below:

1) The networks are implemented in MATLAB/Simulink and used to generate true-value measurements during faults. Measurement noises are added to the true value to create field measurement values.

2) A program for detailed fault analysis is implemented in MATLAB. This program is used to calculate a DOCA for the same contingencies as those modeled in MATLAB/Simulink.

3) The data from 1) are used for obtaining the occurrences of event detection alarm of FRTUs and data polling measurements and compared with DOCA, which is the result of 2). With this process, the final determinations regarding whether OCFs occurred and their locations are made.

The specific configurations of the test networks for MATLAB/Simulink modeling are as follows:

1) Network configuration: The 33-bus network consists of one D/L, and the 118-bus network comprises three D/Ls. The original models have an open-loop topology; however, for this work, the connection points are removed because they are used for fault detection only.

2) Fault location: As shown in Figs. 7 and 8, four and nine fault locations are modeled for the 33- and 118-bus networks, respectively.

3) Fault types: The fault types are chosen as given in Table 3, considering the OCF aspects mentioned in Section II. All faults are assumed to be single-phase faults. For the faults with arcing, a numerical model that was implemented as per the results of actual experiments performed in previous studies is reflected in the MATLAB/Simulink fault model [29]. For the impedance of an HIGF after an OCF, this study refers to the impedance of various materials measured during verification experiments (asphalt: ∼1500 Ω, sidewalk block: ∼2000 Ω) [30]. For the scenarios in which an OCF occurs after a GF (type 6–8), the fault point resistance is set at 30 Ω, which is the maximum impedance considered when setting up protective equipment [31]. However, in fault type 11 wherein only a single-line GF occurs, 50 Ω is additionally tested to examine whether an FP occurs as the fault point resistance increases. In the case of a GF after an OCF

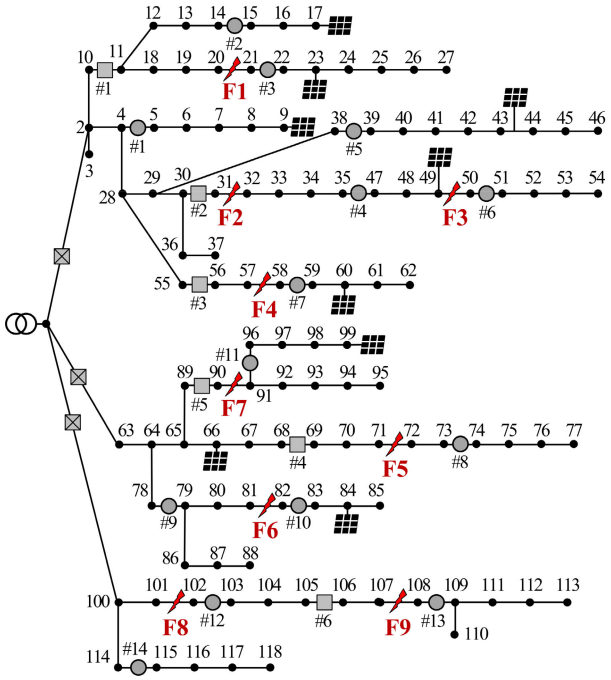

FIGURE 8. 118-bus distribution test system.

TABLE 3. Overall fault scenarios for case studies.

Type	Fault descriptions
1	Maintaining after OCF (no medium contact)
2	Source-side HIGF after OCF (500, 1000, 2000, 3000, 4000, 5000 Ω)
3	Load-side HIGF after OCF (500, 1000, 2000, 3000, 4000, 5000 Ω)
4	Source-side arc after OCF
5	Load-side arc after OCF
6	OCF after GF (0, 15, 30 Ω)
7	OCF (source-side arc) after GF (0, 30 Ω)
8	OCF(load-side arc) after GF (0, 30 Ω)
9	Source-side LIGF after OCF (15, 30, 50 Ω)
10	Load-side LIGF after OCF (15, 30, 50 Ω)
11	GF (0, 15, 30, 50 Ω)

considering a previous study's model of resistance during a GF [32], the minimum fault point resistance is calculated as 15 Ω, and testing is performed up to 50 Ω to validate that the algorithm is valid even when the fault point resistance increases.

The assumptions about fault point resistance in Table 3 are made to calculate the comparison target measurement values. However, the fault point resistance during all real-time operation scenarios cannot be said to match the assumptions in Table 3. Therefore, the measurement difference values according to the fault point for each fault type are examined as presented in Tables 4 and 5. These tests are performed at the same fault locations as the IEEE 33 bus test network,

TABLE 4. Average of difference in measurement values of the FRTU according to fault point resistances (HIGF after OCF).

Fault point resistance		500 Ω	1000 Ω	2000 Ω	3000 Ω	4000 Ω
Difference in measurement of the FRTU	V (%)	0.191	0.085	0.043	0.014	0.006
	I (%)	5.13	3.37	1.70	0.87	0.36
	θ (%)	5.95	3.68	2.12	0.93	0.38

TABLE 5. Average of difference in measurement values of FRTU according to fault point resistances (LIGF after OCF).

Fault point resistance		15–30 Ω	30–50 Ω	15–50 Ω
Difference in measurement values of FRTU	V (%)	1.11	1.57	2.76
	I (%)	3.77	5.62	8.07
	θ (%)	0.10	6.85	7.48

and the measurement data of the FRTU connection point are used. In Table 4, the voltage, current, and PF angle that occur according to fault resistance when there is an HIGF after an OCF are compared with the case where the maximum resistance of 5000 Ω occurs. The test results revealed that in the case of voltage, a maximum difference of 0.191% occurred, and in the case of current and PF angle, differences of 5.13% and 5.95% occurred, respectively. Table 5 presents an analysis of the differences in voltage, current, and PF when comparing a certain fault point resistance and other fault point resistances when an LIGF occurs after an OCF. In the case of 15 Ω, the difference in current with 30 Ω was not large at 3.77%; however, when compared to 50 Ω, there was a relatively large error of 8.07%. In the case of 30 Ω, there was a maximum difference of 6.85% in phase compared to 50 Ω, and the error was smaller than in the case of 15 Ω. In Tables 4 and 5, the error in voltage according to the fault resistance is relatively small, and ultimately it does not exceed the detection criterion when calculating MSE including voltage. Accordingly, it was assumed in this work that the high resistance during the CA was the medium value of 2000 Ω, and the low resistance was 30 Ω, which had the smallest error.

4) FRTU: FRTUs are installed in each piece of protective equipment and SW, and the sampling period of FRTUs is set by setting the simulation time step to 130 μs. In addition, it is assumed that it takes a maximum of 2 s to transmit data to the front-end processor (FEP) after the polling command is received.

5) DER: As for the capacity of the 33-bus DER, 0.8 MW, which is the maximum value among the values suggested by the reference literature [27], is used as the capacity of each DER. In the case of the 118-bus network, the connection varies according to the D/L. For D/L#1 and D/L#2, 9 and 3 MW are connected, assuming 1.5 and 1 MW per PV, respectively. D/L#3 comprises a network with only a load. Moreover, to consider characteristics similar to those of actual power distribution operations, a voltage ride-through function is incorporated from among DER grid codes [33].

6) Protective equipment: For the line protective equipment, it is assumed that an overcurrent relay-based breaker is installed at the feeder start point, and reclosers are placed in the middle of feeders. The protective equipment standards of Korea Electric Power Corporation are used for the minimum pick-up current, time dial setting, and protection coordination [31].

7) Load and lines: The load is connected to all buses, and total active and reactive powers of 3.715 MW and 2.3 MVAr, respectively, are set up for the 33-bus network, while total active and reactive powers of 22.709 MW and 172.041 MVAr are set up for the 118-bus network, respectively. D/L #1, D/L #2, and D/L #3 are set at 10.28 MW and 7.97 Mvar, 7.38 MW and 5.11 Mvar, and 5.05 MW and 3.96 Mvar, respectively. For the line impedance data, the data that are presented in the test network are used.

8) Transformer: The existence of a Yg-Δ connection, which is generally used for DER network connections to prevent the spread of low-voltage-side GFs and suppress harmonics, is assumed, and the transformer for low-voltage loads is set up with a Yg-Yg connection.

9) Measurement error consideration: To reflect the measurement error of the FRTU during faults, an error is assumed according to IEEE C57.13 [24] and IEC 61869 [25]; it is distributed randomly (Gaussian distribution) and used.

A. TESTS USING THE 33-BUS NETWORK

Table 6 presents a comparison of the proposed OCF detection and location method and methods used in previous studies. The proposed method is compared with a current unbalance method [3], multivariate method [5], voltage outage method [7], and voltage unbalance method [8]. The methods used in previous studies are expressed in (13)–(15).

TABLE 6. Results of OCF detection and location for the IEEE 33 test system.

Methods		Current unbalance [3]	Multi-variate [5]	Voltage unbalance [7]	Voltage outage [8]	Proposed method
OCF detection rate according to the fault location (%)	F1	69.9	76.0	47.6	46.9	96.2
	F2	89.6	40.5	36.7	38.5	90.6
	F3	27.6	36.8	30.0	30.8	92.3
	F4	24.1	85.1	33.3	42.3	90.0
	Total	61.8	65.6	42.1	43.5	92.9
FP rate (%)		37.9	15.5	37.9	34.5	6.3
Location rate (%)		-	-	8.6	10.3	92.9

1) The current unbalance method [3] detects the ratio of the positive phase sequence component to the negative phase

sequence component as follows:

$$I_{ub} = \frac{I_2}{I_1}, \tag{13}$$

where I_{ub} is the ratio of the positive phase sequence component to negative phase sequence component, I_1 is the positive sequence of current, and I_2 is negative sequence of current. An OCF is detected if this ratio is greater than 15%.

2) The multivariate detection element method [5] detects OCFs by combining various OFCs such as overvoltage, voltage outage, and current unbalance fluctuations into a decision tree.

3) The voltage outage method [7] uses the voltage drop rate for OCF detection as follows:

$$\Delta V = \frac{|V_{post} - V_{pre}|}{V_{pre}}, \tag{14}$$

where V_{post} is the voltage after the event and V_{pre} is the voltage before the event. An OCF is detected if ΔV is 30% or more.

4) The voltage unbalance method [8] uses the voltage unbalance ratio for detecting an OCF.

$$K = \sqrt{\frac{1-\sqrt{3-6\beta}}{1-\sqrt{3-6\beta}}},\ \beta = \frac{V_{AB}^4 + V_{BC}^4 + V_{AC}^4}{\left(V_{AB}^2 + V_{BC}^2 + V_{AC}^2\right)^2} \tag{15}$$

where K is voltage unbalance rate, V_{AB}, V_{BC}, V_{cb} is the magnitude of line voltages. An OCF is detected if K is 30% or more.

In the proposed method, the individual event alarm of the FRTU criterion for detecting OCFs is set at 6% for voltage by adding the measurement error and the voltage fluctuation rate as mentioned previously. In the case of current, it is set at 15% as per a previous study [3]. Finally, OCF detection based on minimum MSE is set at 7%, considering measurement error and the margin.

Table 6 lists the detection rate, FP rate, and location rate in the previous methods and the proposed method. The detection rate refers to the ratio at which OCFs are classified and detected for all faults. Table 6 reveals that the proposed method improves the detection rate compared to the previous methods regardless of the fault location. In the case of the voltage-based method, when a fault occurred at the end of the line, the detection rate decreased because the voltage was maintained owing to the DERs. In the case of the current unbalance-based method, when the difference between the PV output and the load below the fault point was small, as in the case of fault locations "F3" and "F4" in Fig. 7, the detection rate decreased because the unbalance was low owing to the current supplied by the DERs. The multivariate detection-based method was also found to have a sharply reduced detection rate when the fault occurred at the end of the line because most OFCs had little fluctuation. Particularly in the case of location "F3", which is on the shortest branch line, all the previous methods showed low detection rates, but the proposed method achieved a high detection rate with little difference from those for other locations. This result indicates that the proposed method is effective at detecting faults in networks connected to multiple DERs and at the ends of lines. The FP rate given in Table 6 is the rate at which fault type 11 (GF) was incorrectly judged as an OCF. The proposed method produced only one FP in the single-line GF scenario. As for the other methods, the single-element methods had FP rates of 30% or more when there was a GF fault, and the multivariate method had an FP rate of more than 15%. From these results, it was found that the proposed method had a high detection rate improvement of 27.3%–50.8% and dramatically improved the FN rate (30.2%–65.3%) for faults at the ends of lines and in lines with a high DER connection capacity, which is a weakness of the existing methods. In particular, it was verified that there was a 9.2%–31.6% improvement in FPs for GFs with more than a certain fault resistance that produces fault point load-side measurement value fluctuations similar to those of OCFs. In addition, location rates were compared. Previous studies [3], [5] only proposed detection methods, while some studies [7], [8] estimated locations by common topology searches in the source-side direction of OCF detection equipment. The location rates were calculated as the ratio of successful locations out of all OCF cases. The proposed method showed good results with a location rate of 92.9%. The previous studies [7], [8] showed poor location rates of 8.6% and 10.3% because many topology searches failed because of the DERs and the FNs of FRTUs.

To determine whether fault locations can be classified as per MSE, Fig. 9 presents the measurement values during OCFs in the source- and load-side sections of the SW (#1, #2, #4, #6) installation point nearest to each fault location. Fig. 9 shows the voltage (■), current (◆), and PF (●) when a fault occurs in the source-side section of the SW as well as the voltage (■), current (◆), and PF (●) when a fault occurs in the load-side section. When high-resistance faults occurred after OCFs in the source- and load-side sections of SW#1, the voltage, current, and PF patterns were similar at other SWs, but current value differences occurred in the FRTUs of CB, RC#2, and SW#6. Furthermore, in the case of GFs after OCFs, there was a difference in the current measurements at CB, SW#1, RC#2, and SW#6 as well as a difference in the PF measurement values at RC#2 and SW#6. In the other graphs as well, if the fault section changes, there is certainly at least one FRTU that shows a difference in at least one of the three measurement elements. Therefore, it is possible to perform location because a difference occurs in the MSE values at both ends of the FRTU section when a fault occurs.

To verify the possibility of distinguishing OCFs from other events, the FRTU measurement values during GFs and OCFs at designated fault locations in the IEEE 33 bus are compared as shown in Fig. 10. In the graph, the light-colored marks show the voltage, current, and PF during an OCF, and the regular marks show the measurement values during a GF. In the case of fault location "F1" in Fig. 7, the voltage measurement values of the FRTU connected to the load side of the fault point showed similar patterns during the OCF

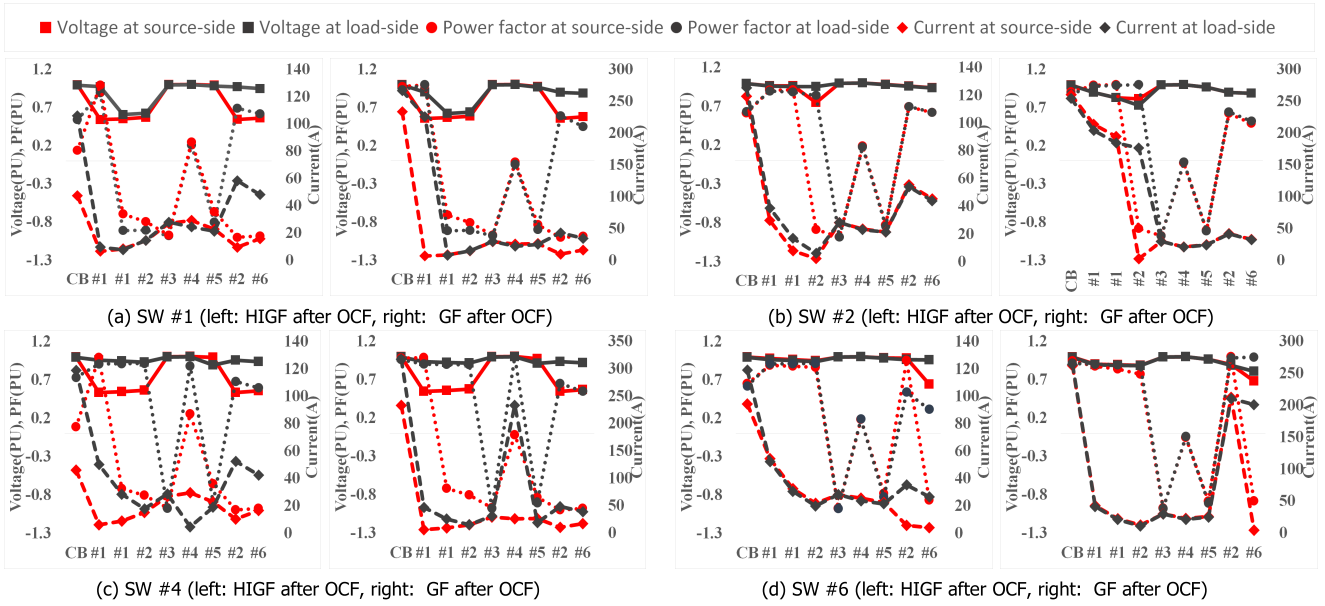

(a) SW #1 (left: HIGF after OCF, right: GF after OCF)

(b) SW #2 (left: HIGF after OCF, right: GF after OCF)

(c) SW #4 (left: HIGF after OCF, right: GF after OCF)

(d) SW #6 (left: HIGF after OCF, right: GF after OCF)

FIGURE 9. Comparison of measured values of faults at both sides of the SW (From the left: SW#1, RC#1, SW#2, SW#3, SW#4, SW#5, RC#2, and SW#6).

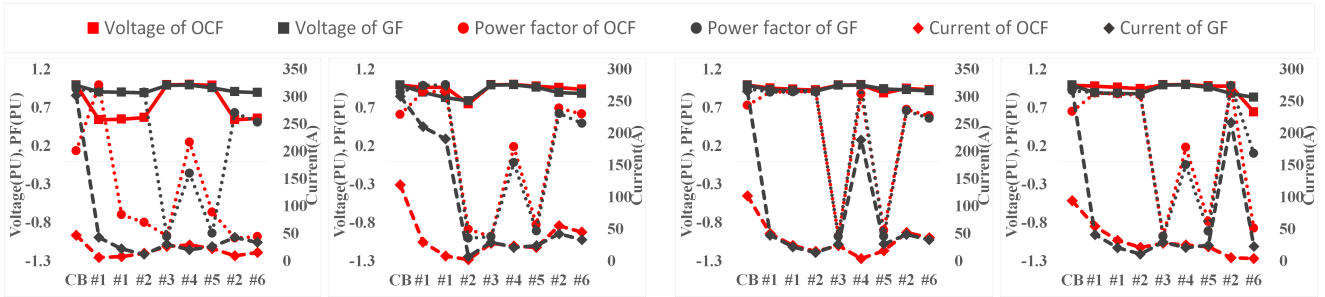

(a) Fault location F1 (OCF, GF)

(b) Fault location F2 (OCF, GF)

(c) Fault location F3 (OCF, GF)

(d) Fault location F4 (OCF, GF)

FIGURE 10. Comparison of measured values of each FRTU when OCF or GF occurs.

and the GF. However, there were differences in current and PF measurement values at the FRTU connected to the source side of the fault point. In the case of fault location "F4," there was no considerable difference in PF, but there were large differences in the current measurement values at CB and RC#2. In addition, at all fault locations, there was at least one FRTU where differences in the OCF and GF measurement values occurred.

B. PERFORMING TESTS USING THE 118-BUS NETWORK

This study analyzes the detection rate and FP rate according to adjustments in detection criterion (ε) of in. (11) for the network as given in Table 7. In the test results, at 6% or less, there were no FPs, but the detection rate was relatively low. The FP rate was the same at 7% and 8%, but the detection rate increased at 8%. At 9% and above, the detection rate increased, but the FP rate increased sharply. On the basis of these results, the detection criterion was set at 8%; Table 8 presents the results of the analysis of each feeder. As the DER connections became more numerous, the detection rate decreased, but the overall detection rate for each D/L was high, and the difference due to the DER connections was small. Most of the location attempts were successful when an OCF was detected. The FP rate for GFs was also low, and FPs only occurred in 2 out of 36 scenarios.

To verify reliability in an actual network, tests were performed by changing the polling time of the FRTUs as given in Table 9. Maximum delay times were assumed, and an FRTU that transmitted polling commands randomly was selected. Maximum delay times of 1.5, 2, 3, and 4 s were assumed, given the processing times from the FRTU to the central office terminal (COT), from the COT to the FEP, and from the FEP to the DMS. The results are presented in Table 9. When the communication delay was 2 s, the detection rate was high and showed no difference compared to the existing results. When the communication delay was 3 s or more, the detection rate decreased slightly because of the difference in measurement times, data transmissions in an outage due to the operation of the protective equipment, etc. However, a high detection rate was maintained.

To verify the effects of communication failures, the detection rate according to the wired/wireless ratio of FRTUs is examined; the corresponding results are given in Table 10. In FRTU wired communications, fiber-optic cables were

TABLE 7. Detection and FP rate according to detection criteria.

Detection criteria (%)	5	6	7	8	9	10
Detection rate (%)	84.9	89.1	92.9	94.4	96.6	97.7
FP rate (%)	0	0	5.56	5.56	13.9	27.8

TABLE 8. Results of OCF detection and location for the 118-bus test system.

D/Ls	1	2	3	Average
Detection rate (%)	91.6	94.4	100	94.4
FP rate (%)	6.25	8.3	0	5.6
Location rate (%)	96.4	98.1	100	97.8

TABLE 9. Test results considering communication delay.

Comm. delay time		1.5	2	3	4
Detection rate (%)	D/L 1	92.5	91.6	89.1	87.5
	D/L 2	94.4	94.4	92.2	91.1
	D/L 3	100	100	96.4	89.3
	Total	94.8	94.4	91.8	89.1

used, and it was assumed that almost no communication failures occurred. In FRTU wireless communications, frequency-based methods and wireless local area network were used, and a communication failure rate of ∼10% was assumed. In Korea, most communications are performed via wires, but in countries with inadequate infrastructure investment, the ratio of wireless communications is higher, and the effect of communication failures is greater. To examine this, Korea's wired/wireless communication ratio of 85:15 was compared with ratios of 50:50 and 15:85. Although communication failures occurred as the wireless ratio increased, the detection rate did not change significantly, and a single communication failure had almost no effect. This result implies that the proposed method is robust against communications failures.

Finally, the time taken to create contingency cases from an actual DMS was measured to determine the time taken when the proposed algorithm was installed. All simulations were performed on a PC with an Intel core i7 3.4-GHz CPU and 32-GB RAM. When CA was performed with the algorithm, it took 0.77 and 9.04 s in the case of the IEEE 33 bus and 118 bus, respectively. As mentioned previously, the CA is performed in the non-real-time study mode, and other than the initial startup, it is only performed for D/Ls that have undergone topology changes. Therefore, this level of time consumption will not be a significant issue when applying the proposed method.

TABLE 10. Test results considering communication failures.

Wired and wireless ratio		85:15	50:50	15:85
Detection rate (%)	D/L 1	91.6	91.6	90.8
	D/L 2	94.4	93.3	91.1
	D/L 3	100	98.2	96.4
	Total	94.4	93.6	92.1

V. CONCLUSION

This study proposes a contingency analysis-based OCF detection and location method for power distribution networks.

Following are the main conclusions of this study:

1) By comparing the distance between the entire measurement set and DOCA, the proposed method significantly improves the OCF detection rate by 27.3%–50.8% compared to existing methods that use a specific detection element. In addition, the proposed method improves FNs for faults in lines with a high DER connection capacity and line ends, which is a weakness of existing methods.

2) Using the weights based on the magnitude variation of the comparison elements when calculating the distance between the DOCA and FRTU sets, the proposed method significantly reduces the occurrence of FPs in other events such as GFs by 9.2%–31.6%. Improving upon FPs, which are a type of false alarm, is very important for operations. Repeated false alarms are significant in that they can lead to a "Cry Wolf Effect" in which alarms for actual events are ignored because operators and field crews are repeatedly overworked and ignore repeated alarms. In addition, tests that reflect realistic conditions such as FRTU measurement errors, time delays due to polling commands, and communications failures due to the wired/wireless communication ratio are performed. Accordingly, the proposed method is confirmed to be robust under a variety of realistic conditions, proving its adaptability to actual power-distribution networks.

3) In the location of OCFs, the proposed approach shows better results compared by 82.6%–84.3% to previous methods. OCFs are permanent faults, and they must be dealt with by dispatching field crews, which makes it crucial to locate them in comparison with other events. Therefore, the proposed algorithm, which performs detection and location simultaneously, will be able to increase reliability by enabling rapid responses during actual operations.

4) The proposed algorithm uses data that are commonly possessed by power companies and the typical FRTU measurement values. Therefore, it is practical in that there is no need for special investments in facilities, and it can be universally applied to power distribution network operation systems that are equipped with basic infrastructure. This paper proposes an aperiodic screening method. However, additional research is required on the criteria for selecting the target D/Ls that need CA. It is possible to determine the risk of forest fires from weather data and predict situations in

which damages increase when OCFs occur. In addition, the accident rates in a distributed power network increase when the network is newly installed or when its lifespan is expiring and the time for replacement is approaching [34]. These facts could be used to adjust the period and scope of the analysis and reduce the overall time taken by contingency analysis.

As DER connections rapidly increase, fault detection and location are becoming increasingly complex. However, the lack of timely and commensurate investments in facilities is a common problem that must be resolved to protect power distribution networks. Therefore, it is important to devise methods that can handle power distribution networks that create changes within the current infrastructure and systems, and the use of the proposed method will be effective in reducing damages caused by OCFs in current power-distribution networks.

REFERENCES

[1] G. Bade. (Nov. 2018). *PG&E Reports Second Line Fault in Camp Fire Area*. [Online]. Available: https://www.utilitydive.com/news/

[2] Y.-S. Ko, "A self-isolation method for the HIF zone under the network-based distribution system," *IEEE Trans. Power Del.*, vol. 24, no. 2, pp. 884–891, Apr. 2009.

[3] D. K. J. S. Jayamaha, I. H. N. Madhushani, R. S. S. J. Gamage, P. P. B. Tennakoon, J. R. Lucas, and U. Jayatunga, "Open conductor fault detection," in *Proc. Moratuwa Eng. Res. Conf. (MERCon)*, Moratuwa, Sri Lanka, May 2017, pp. 363–367.

[4] A. Wontroba, A. P. Morais, G. J. Cardoso, J. P. A. Vieira, P. E. Farias, M. Gallas, and J. P. Rossini, "High-impedance fault detection on downed conductor in overhead distribution networks," *Electr. Power Syst. Res.*, vol. 211, Oct. 2022, Art. no. 108216.

[5] J.-S. Hong, S.-Y. Hyun, Y.-W. Lee, J.-H. Choi, S.-J. Ahn, and S.-Y. Yun, "Detection of open conductor fault using multiple measurement factors of feeder RTUs in power distribution networks with DGs," *IEEE Access*, vol. 9, pp. 143564–143579, 2021.

[6] V. H. Makwana and B. R. Bhalja, "A new digital distance relaying scheme for series-compensated double-circuit line during open conductor and ground fault," *IEEE Trans. Power Del.*, vol. 27, no. 2, pp. 910–917, Apr. 2012.

[7] L. Garcia-Santander, P. Bastard, M. Petit, I. Gal, E. Lopez, and H. Opazo, "Down-conductor fault detection and location via a voltage based method for radial distribution networks," *IEE Proc., Gener., Transmiss. Distrib.*, vol. 152, no. 2, p. 180, 2005.

[8] F. L. Vieira, P. H. M. Santos, J. M. C. Filho, R. C. Leborgne, and M. P. Leite, "A voltage-based approach for series high impedance fault detection and location in distribution systems using smart meters," *Energies*, vol. 12, no. 15, p. 3022, Aug. 2019.

[9] E. M. Esmail, M. M. Elgamasy, T. A. Kawady, A.-M.-I. Taalab, N. I. Elkalashy, and M. A. Elsadd, "Detection and experimental investigation of open conductor and single-phase Earth return faults in distribution systems," *Int. J. Electr. Power Energy Syst.*, vol. 140, Sep. 2022, Art. no. 108089.

[10] J. Li, Y. Liu, C. Li, D. Zeng, H. Li, and G. Wang, "An FTU-based method for locating single-phase high-impedance faults using transient zero-sequence admittance in resonant grounding systems," *IEEE Trans. Power Del.*, vol. 37, no. 2, pp. 913–922, Apr. 2022.

[11] M. Michalik, M. Lukowicz, W. Rebizant, S.-J. Lee, and S.-H. Kang, "New ANN-based algorithms for detecting HIFs in multigrounded MV networks," *IEEE Trans. Power Del.*, vol. 23, no. 1, pp. 58–66, Jan. 2008.

[12] H.-G. Yeh, S. Sim, and R. J. Bravo, "Wavelet and denoising techniques for real-time HIF detection in 12-kV distribution circuits," *IEEE Syst. J.*, vol. 13, no. 4, pp. 4365–4373, Dec. 2019.

[13] B. K. Chaitanya, A. Yadav, and M. Pazoki, "An intelligent detection of high-impedance faults for distribution lines integrated with distributed generators," *IEEE Syst. J.*, vol. 14, no. 1, pp. 870–879, Mar. 2020.

[14] J. Che, T. Kim, S. Pyo, J. Park, B. An, and T. Park, "Prevention of wildfires using an AI-based open conductor fault detection method on overhead line," *Energies*, vol. 16, no. 5, p. 2366, Mar. 2023.

[15] H. Xu, X. Wang, J. Huang, F. Zhang, and F. Chu, "Semi-supervised multi-sensor information fusion tailored graph embedded low-rank tensor learning machine under extremely low labeled rate," *Inf. Fusion*, vol. 105, May 2024, Art. no. 102222.

[16] J. B. Thomas, S. G. Chaudhari, K. V. Shihabudheen, and N. K. Verma, "CNN-based transformer model for fault detection in power system networks," *IEEE Trans. Instrum. Meas.*, vol. 72, pp. 1–10, 2023.

[17] X. Wang, T. Ding, and W. Xu, "An open conductor condition monitoring scheme using natural voltage and current disturbances," *IEEE Trans. Power Del.*, vol. 34, no. 3, pp. 1193–1202, Jun. 2019.

[18] S. H. Mortazavi, Z. Moravej, and S. M. Shahrtash, "A searching based method for locating high impedance arcing fault in distribution networks," *IEEE Trans. Power Del.*, vol. 34, no. 2, pp. 438–447, Apr. 2019.

[19] Z. Lin, Z. Hu, and Y. Song, "Distribution network expansion planning considering $N-1$ criterion," *IEEE Trans. Power Syst.*, vol. 34, no. 3, pp. 2476–2478, May 2019.

[20] Q. Zou, F. Luo, and T. Zhang, "An incidence matrix based analytical method of N-1 contingency parallel analysis of main transformers in distribution networks," *CSEE J. Power Energy Syst.*, early access, May 6, 2022, doi: 10.17775/CSEEJPES.2021.01490.

[21] S. J. Simmons, "Breadth-first trellis decoding with adaptive effort," *IEEE Trans. Commun.*, vol. 38, no. 1, pp. 3–12, Jan. 1990.

[22] J. J. Grainger, W. D. Stevenson, and G. W. Chang, *Power System Analysis*, 2nd ed., New York, NY, USA: McGraw-Hill, 2016, pp. 422–430.

[23] J.-S. Hong, G.-D. Sim, J.-H. Choi, S.-J. Ahn, and S.-Y. Yun, "Fault location method using phasor measurement units and short circuit analysis for power distribution networks," *Energies*, vol. 13, no. 5, p. 1294, Mar. 2020.

[24] *IEEE Standard Requirements for Instrument Transformers*, Standard C57.13, 2016.

[25] *IEC Instrument Transformers—Part 2: Additional Requirements for Current Transformers*, Standard 61869, IEC, 2012.

[26] *IEEE Standard for Interconnection and Interoperability of Distributed Energy Resources With Associated Electric Power Systems Interfaces*, IEEE Standard IEEE 1547, 2018.

[27] S. H. Dolatabadi, M. Ghorbanian, P. Siano, and N. D. Hatziargyriou, "An enhanced IEEE 33 bus benchmark test system for distribution system studies," *IEEE Trans. Power Syst.*, vol. 36, no. 3, pp. 2565–2572, May 2021.

[28] D. Zhang, Z. Fu, and L. Zhang, "An improved TS algorithm for loss-minimum reconfiguration in large-scale distribution systems," *Electr. Power Syst. Res.*, vol. 77, nos. 5–6, pp. 685–694, Apr. 2007.

[29] S.-Y. Hyun, J.-S. Hong, S.-Y. Yun, C.-H. Kim, and Y. Lee, "Arc modeling and kurtosis detection of fault with arc in power distribution networks," *Appl. Sci.*, vol. 12, no. 6, pp. 2777–2793, Mar. 2022.

[30] Y.-B. Jung, W.-S. Choi, Y.-S. Jeon, and B.-S. Lee, "Development of method for detecting high impedance fault," KEPCO, Naju, South Korea, Tech. Rep. R11DA01, Sep. 2013, pp. 90–93.

[31] *Guidelines for Distribution Network Protection*, KEPCO, Naju, South Korea, Oct. 2008.

[32] V. D. Andrade and E. Sorrentino, "Typical expected values of the fault resistance in power systems," in *Proc. IEEE/PES Transmiss. Distrib. Conf. Expo., Latin Amer. (TD-LA)*, Sao Paulo, Brazil, Nov. 2010, pp. 602–609.

[33] *Technical Standards of the Distributed Energy Resource Connection in Power Distribution System*, KEPCO, Naju, South Korea, 2021.

[34] G. Klutke, P. C. Kiessler, and M. A. Wortman, "A critical look at the bathtub curve," *IEEE Trans. Rel.*, vol. 52, no. 1, pp. 125–129, Mar. 2003.

GI-DO SIM (Student Member, IEEE) received the B.S. and M.S. degrees in electrical engineering from Chonnam National University, Gwangju, South Korea, in 2018 and 2020, respectively, where he is currently pursuing the Ph.D. degree with the Department of Electrical Engineering. His research interests include distribution network protection technologies, fault analysis, fault detection and location, and protection coordination optimization.

HYO-SEOP IM (Student Member, IEEE) received the B.S. degree in electrical engineering from Chonnam National University, Gwangju, South Korea, in 2022, where he is currently pursuing the integrated Ph.D. degree with the Department of Electrical Engineering. His research interests include distributed generation and operating distribution systems.

JOON-HO CHOI (Senior Member, IEEE) received the B.S., M.S., and Ph.D. degrees in electrical engineering from Soongsil University, Seoul, South Korea, in 1996, 1998, and 2002, respectively. Since 2003, he has been a Professor with Chonnam National University, Gwangju, South Korea. His research interests include operation and control strategies of distributed generation and operation algorithms of smart grids.

SEON-JU AHN (Member, IEEE) received the B.S., M.S., and Ph.D. degrees in electrical engineering from Seoul National University, Seoul, South Korea, in 2002, 2004, and 2009, respectively. He is currently a Professor with Chonnam National University, Gwangju, South Korea. His current research interests include power quality, distributed energy resources, microgrids, smart grids, and real-time simulation.

SANG-YUN YUN (Member, IEEE) received the B.S., M.S., and Ph.D. degrees in electrical engineering from Soongsil University, Seoul, South Korea, in 1996, 1998, and 2002, respectively. From 2002 to 2009, he was a Senior Researcher with the Electrotechnology Research and Development Center, LSIS, Cheongju, South Korea. From 2009 to 2016, he was a Senior Researcher at the KEPCO Research Institute, Daejeon, South Korea. He is currently a Professor with the Department of Electrical Engineering, Chonnam National University, Gwangju, South Korea. His research interests include the design of EMS, DMS, and MGMS as well as protection technologies for active distribution networks.